Modeling Scattering Fields from an Infinitely Long PEC Cylinder with Different Cross Sections Using 2D MoM

Xiaojun Zhu

December 13, 2021

Abstract

In this project, we developed a 2D method of moments (MoM) program to model the transverse magnetic (TM) and transverse electric (TE) fields scattering from an infinitely long PEC cylinder with various cross-sections. We first briefly reviewed the formulation of 2D electric field integral equation (EFIE) and magnetic field integral equation (MFIE) for inhomogeneous Helmholtz equations, and also introduced the key procedures of the MoM implementation. The MoM program was developed in Matlab using the triangular mesh generated in *pdetool*. The field distributions of the circular cylinder from the MoM for both TE and TM polarizations were validated by comparing the analytical solutions with different radii. A good agreement between the numerical and analytical solutions was obtained.

1 Introduction

The method of moments (MoM), also known as moment method (MM) or boundary element method (BEM), transforms the governing equation of a boundary-value problem into a matrix equation similar to the finite element method (FEM). However, instead of solving the partial differential equations related to Maxwell's equation when using the finite difference method (FDM) and FEM, the solutions of Maxwell's equation can be obtained by solving an integral equation derived from Maxwell's equation [1].

Although similarities exist compared to the FEM, such as using *weighted residual method*, the MoM only discretizes the surface of the object of interest instead of the entire volume of the object [1]. This reduction in dimensionality can be substantial for large problems. The MoM also has much larger function space for test/basis function. For example, it could apply a zero-order function since there is no need to evaluate derivatives. Besides, there is also no need for artificial boundary conditions in MoM. This, together with the reduction in dimensionality, is advantageous for problems like PEC scattering despite other features of the MoM.

For a PEC object scattering problem, the inhomogeneous Helmholtz equation may be solved analytically for describing waves scattered by an infinitely long PEC cylinder with a circular cross-section via wave transformation [1]. However, for other cross-sections such as square, there may not be an analytical solution for the inhomogeneous Helmholtz equation. In this project, a 2D MoM was developed in Matlab to simulate the TM and TE scattering from an infinitely long PEC cylinder of different cross-sections that are circular, square, and irregular. The *pdetool* was used to generate discretized segments on the boundary of each cross-section. The analytical solutions of the circular PEC cylinder were used for validation.

In the next section, we briefly introduce the 2D electric field integral equation and 2D magnetic field integral equation for calculating the TM and TE scattering fields, respectively, from an infinitely long PEC cylinder. The key procedures of the MoM implementation are introduced. Section 3 gives the results and discussions including the result validation by using analytical solutions. The last section gives the conclusions and possible future work.

2 Methods

We first review the key procedures of deriving the 2D electric field integral equation (EFIE) and 2D magnetic field integral equation (MFIE) for numerically solving inhomogeneous Helmholtz equations for both TM and TE polarizations, respectively. The presented MoM method applies point-matching for simplicity [1]. Some important procedures of the MoM implementation in Matlab are also introduced.

We consider a 2D object in free space as illustrated in Figure 1. Exterior to the object, the inhomogeneous Helmholtz equation is given by

$$\nabla^2\varphi(\mathbf{r}) + k_0^2\varphi(\mathbf{r}) = f(\mathbf{r}) \quad \mathbf{r} \in \Omega_\infty \tag{1}$$

where k_0 is the wavenumber and $f(\mathbf{r})$ is the source producing the scalar wave. The radiation condition can be given as

$$\sqrt{r}\left[\frac{\partial\varphi(\mathbf{r})}{\partial r} + jk_0\varphi(\mathbf{r})\right] = 0 \quad r \to \infty. \tag{2}$$

To derive an integral equation for this 2D scattering problem, We introduce the free-space Green's function that satisfies the inhomogeneous Helmholtz equation

$$\nabla^2 G_0(\mathbf{r}, \mathbf{r}') + k_0^2 G_0(\mathbf{r}, \mathbf{r}') = -\delta(\mathbf{r} - \mathbf{r}') \tag{3}$$

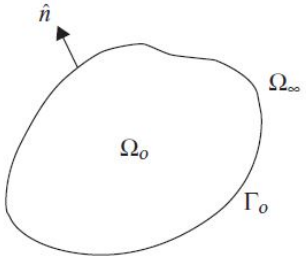

Figure 1: 2D object in free space [1].

where the free-space Green's function is given by

$$G_0(\mathbf{r},\mathbf{r}') = \frac{1}{4j} H_0^{(2)}(k_0\,|\mathbf{r}-\mathbf{r}'|) \tag{4}$$

where $H_0^{(2)}$ is the zeroth-order Hankel function of the second kind. Using (1)-(4) the mathematical representation of Huygens' principle for scalar fields can be given [1]:

$$\varphi^{\text{inc}}(\mathbf{r}) + \oint_{\Gamma_0} \left[\varphi(\mathbf{r}')\frac{\partial G_0(\mathbf{r},\mathbf{r}')}{\partial n'} - G_0(\mathbf{r},\mathbf{r}')\frac{\partial \varphi(\mathbf{r}')}{\partial n'}\right] d\Gamma' = \begin{cases} \varphi(\mathbf{r}), & \mathbf{r}\in\Omega_\infty \\ 0, & \mathbf{r}\in\Omega_0. \end{cases} \tag{5}$$

In the cylindrical coordinates, by using semicircular deformation for the integral in (5) [1], (5) can be simplified as

$$\varphi^{\text{inc}}(\mathbf{r}) + \lim_{\varepsilon\to 0}\int_{\Gamma_0-2\varepsilon} \left[\varphi(\mathbf{r}')\frac{\partial G_0(\mathbf{r},\mathbf{r}')}{\partial n'} - G_0(\mathbf{r},\mathbf{r}')\frac{\partial \varphi(\mathbf{r}')}{\partial n'}\right] d\Gamma' = \frac{1}{2}\varphi(\mathbf{r}),\ \mathbf{r}\in\Gamma_0 \tag{6}$$

where ε is the radius of a semicircle centered at $\mathbf{r}$.

2.1 2D Electric field integral equation

For TM waves, the electric field satisfies the inhomogeneous Helmholtz equation

$$\nabla^2 E_z(\mathbf{r}) + k_0^2 E_z(\mathbf{r}) = jk_0 Z_0 J_{i,z}(\mathbf{r}) \quad \mathbf{r}\in\Omega_\infty \tag{7}$$

where $J_{i,z}(\mathbf{r})$ is the source of the incident field, $k_0 = k = 2\pi/\lambda$ is the wavenumber (λ: wavelength of the incident field), and Z_0 is the impedance of free space. The boundary conditions on the surface of the PEC cylinder can be given as

$$E_z(\mathbf{r}') = 0 \quad \mathbf{r}'\in\Gamma_0 \tag{8}$$

$$\frac{\partial E_z(\mathbf{r}')}{\partial n'} = jk_0 Z_0 J_{s,z}(\mathbf{r}') \quad \mathbf{r}' \in \Gamma_0 \tag{9}$$

where $J_{s,z}(\mathbf{r}')$ is the surface current density generated by the incident field. Substituting (7)-(9) into (6), one may obtain the electric-field integral equation (EFIE) [1]:

$$E_z^{\text{inc}}(\mathbf{r}) - jk_0 Z_0 \int_{\Gamma_0} G_0(\mathbf{r}, \mathbf{r}') J_{s,z}(\mathbf{r}') d\Gamma' = 0, \quad \mathbf{r} \in \Gamma_0. \tag{10}$$

To solve (10) numerically, we may divide Γ_0 into small segments, as shown in Figure 2, and approximate $J_{s,z}(\mathbf{r}')$ over each segment as a constant. Using a point matching or point collection procedure (testing with a delta function) one may obtain

$$\sum_{n=1}^{N} Z_{mn} J_{z,n} = V_m \quad m = 1, 2, ...N \tag{11}$$

where

$$Z_{mn} = jk_0 Z_0 \int_{s_n} G_0(\mathbf{r}_m, \mathbf{r}') d\Gamma' \tag{12}$$

$$V_m = E_z^{\text{inc}}(\mathbf{r}_m) \tag{13}$$

where s_n is the nth segment length and $\mathbf{r}_m$ represents the center of the mth segment. Using the midpoint integration and the small-argument approximation for the Hankel function, (12) can be evaluated by

$$Z_{mn} = \begin{cases} \frac{1}{4} k_0 Z_0 s_n H_0^{(2)}(k_0 |\mathbf{r}_m - \mathbf{r}_n|), & m \neq n \\ \frac{1}{4} k_0 Z_0 s_n \left[1 - j\frac{2}{\pi} \ln\left(\frac{k_0 \gamma s_n}{4e}\right)\right], & m = n \end{cases} \tag{14}$$

where $\gamma = 1.781$ and $e \approx 2.7183$. Once $J_{z,n}$ (or $J_{s,z}(\mathbf{r}')$) is calculated by solving (11), the electric field anywhere in Ω_∞ can be evaluated by using (5) which, in this case, is given by

$$E_z(\mathbf{r}) = E_z^{\text{inc}}(\mathbf{r}) - jk_0 Z_0 \oint_{\Gamma_0} G_0(\mathbf{r}, \mathbf{r}') J_{s,z}(\mathbf{r}') d\Gamma' \quad \mathbf{r} \in \Omega_\infty. \tag{15}$$

2.2 2D Magnetic field integral equation

For TE waves, the magnetic field satisfies the inhomogeneous Helmholtz equation

$$\nabla^2 H_z(\mathbf{r}) + k_0^2 H_z(\mathbf{r}) = -\left[\nabla \times \mathbf{J}_i(\mathbf{r})\right]_z \qquad \mathbf{r} \in \Omega_\infty \tag{16}$$

where $\nabla \times \mathbf{J}_i(\mathbf{r})$ is the source of the incident field. The boundary conditions on the surface of the PEC cylinder can be given as

$$H_z(\mathbf{r}') = -J_{s,t}(\mathbf{r}') \qquad \mathbf{r}' \in \Gamma_0 \tag{17}$$

$$\frac{\partial H_z(\mathbf{r}')}{\partial n'} = 0 \qquad \mathbf{r}' \in \Gamma_0 \tag{18}$$

where $J_{s,t}(\mathbf{r}')$ is the surface current density generated by the incident field. Substituting (16)-(18) into (6), one may obtain the magnetic-field integral equation (MFIE) [1]:

$$H_z^{\text{inc}}(\mathbf{r}) - \lim_{\varepsilon \to 0} \int_{\Gamma_0 - 2\varepsilon} \frac{\partial G_0(\mathbf{r}, \mathbf{r}')}{\partial n'} J_{s,t}(\mathbf{r}') d\Gamma' = \frac{1}{2} J_{s,t}(\mathbf{r}), \ \mathbf{r} \in \Gamma_0. \tag{19}$$

To solve (19) numerically, one may divide Γ_0 into small segments and approximate $J_{s,t}(\mathbf{r}')$ over each segment as a constant. Similarly, using a point matching procedure we may obtain

$$\sum_{n=1}^{N} Z_{mn} J_{t,n} = V_m \quad m = 1, 2, ...N \tag{20}$$

where

$$Z_{mn} = \lim_{\varepsilon \to 0} \int_{s_n - 2\varepsilon} \frac{\partial G_0(\mathbf{r}_m, \mathbf{r}')}{\partial n'} d\Gamma' - \frac{1}{2}\delta_{mn} \tag{21}$$

$$V_m = H_z^{\text{inc}}(\mathbf{r}_m) \tag{22}$$

where $\delta_{mn} = 1$ for $m = n$ and $\delta_{mn} = 0$ for $m \neq n$. Substituting (4) into the integral in (21) the derivative may be evaluated by [1]

$$\frac{\partial G_0(\mathbf{r}_m, \mathbf{r}')}{\partial n'} = \frac{1}{4j} \hat{n}' \cdot \nabla' H_0^{(2)}(k_0 \left|\mathbf{r}_m - \mathbf{r}'\right|) = \frac{k_0}{4j} H_1^{(2)}(k_0 \left|\mathbf{r}_m - \mathbf{r}'\right|) \frac{\hat{n}' \cdot (\mathbf{r}_m - \mathbf{r}')}{\left|\mathbf{r}_m - \mathbf{r}'\right|} \tag{23}$$

where $H_1^{(2)}$ is the first-order Hankel function of the second kind. Using (23) and the midpoint integration, (21) can be evaluated by

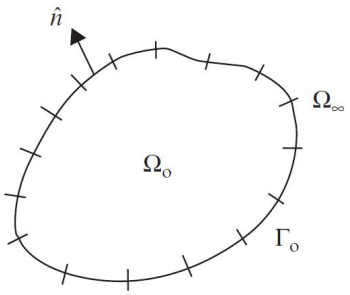

Figure 2: Contour Γ_0 divided into short segments [1].

$$Z_{mn} = \begin{cases} \frac{k_0 s_n}{4j} H_1^{(2)}(k_0 \left|\mathbf{r}_m - \mathbf{r}_n\right|) \frac{\hat{n}' \cdot (\mathbf{r}_m - \mathbf{r}_n)}{|\mathbf{r}_m - \mathbf{r}_n|}, & m \neq n \\ -\frac{1}{2}, & m = n. \end{cases} \tag{24}$$

Once $J_{t,n}$ (or $J_{s,t}(\mathbf{r}')$) is calculated by solving (20), the magnetic field in Ω_∞ can be evaluated by using (5) which, in this case, is given by

$$H_z(\mathbf{r}) = H_z^{\text{inc}}(\mathbf{r}) - \oint_{\Gamma_0} \frac{\partial G_0(\mathbf{r}, \mathbf{r}')}{\partial n'} J_{s,t}(\mathbf{r}') d\Gamma' \quad \mathbf{r} \in \Omega_\infty. \tag{25}$$

2.3 MoM implementation

As the first step, the *pdetool* in Matlab was used to generate 2D triangular mesh for the discretization of Γ_0. Figure 3 shows the triangular mesh cells for a 2D irregular cross-section of a PEC cylinder generated from the *pdetool*. Unlike FEM, we only need the discretized edges on Γ_0 and the coordinates of the corresponding boundary nodes for the MoM. The boundary nodes can be easily extracted from the generated file from *pdetool* and aliened to the associated edges. Then, s_n and r_m (or r_n) in (14) and (24) can be evaluated handily using the Cartesian coordinates from the *pdetool*. For the incident fields, we consider nondimensionalized fields for simplicity and comparison. We may define the non-dimensional V for the incident field which is applicable for both TM and TE cases. Then V_m in (13) and (22) can be calculated by using:

$$V = e^{-jk_0 x}. \tag{26}$$

Figure 4 shows the incident field propagating in the x direction. Once $J_{s,z}(r_m)$ is solved, one may use (15) in discretized form to calculate and $E_z(\mathbf{r})$ which is given by

$$E_z(\mathbf{r}) = E_z^{\text{inc}}(\mathbf{r}) - jk_0 Z_0 \sum_{m=1}^{M} G_0(\mathbf{r}, \mathbf{r_m}) J_{s,z}(\mathbf{r_m}) s_m \quad \mathbf{r} \in \Omega_\infty \tag{27}$$

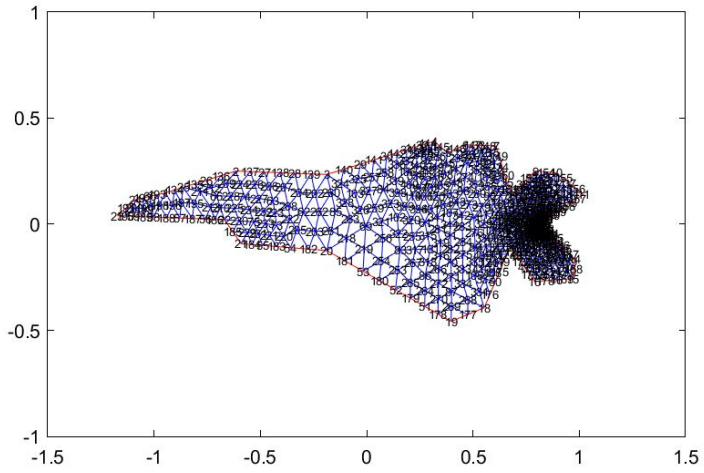

Figure 3: Triangular mesh for a somewhat irregular cross section drawn by hand.

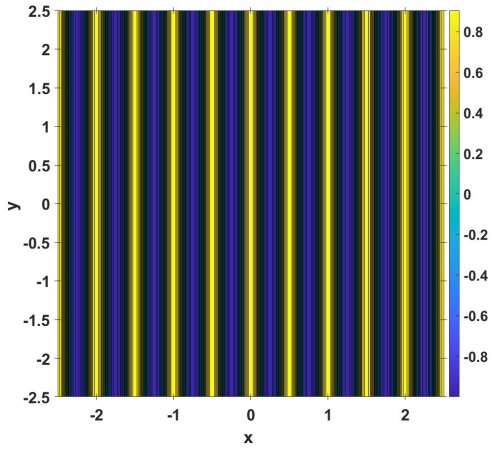

Figure 4: Incident field propagating in the x-direction.

where M is the number of the segments on the boundary and s_m is the mth segment length. Similarly, $H_z^{sc}(\mathbf{r})$ and $H_z(\mathbf{r})$ may be evaluated by using (25) in discretized form that is given by

$$H_z(\mathbf{r}) = H_z^{\text{inc}}(\mathbf{r}) - \sum_{m=1}^{M} \frac{\partial G_0(\mathbf{r}, \mathbf{r_m})}{\partial n'} J_{s,z}(\mathbf{r_m}) s_m \quad \mathbf{r} \in \Omega_\infty. \tag{28}$$

It should be noted that when assembling matrix $[Z_{mn}]$ in (24) using (23) $\hat{n}'$ is the unit vector for $\mathbf{r}'$ (or $\mathbf{r}_n$ as shown in (24)). Thus, it may be evaluated by using $\hat{n}' = \mathbf{r}_n / |\mathbf{r}_n|$. The same rule is applied in (28).

3 Results and Discussions

3.1 MoM results for various cross sections

For the circular PEC cylinders, the radius $R = 0.5$m was fixed, while different wavelengths λ were applied for comparison. Figure 5 and 6 show the results of the scattering fields E_z^{sc} and H_z^{sc} and total fields E_z and H_z for circular PEC cylinders with $\lambda = R$ and $0.5R$, respectively. For the same PEC object, the scattered fields become stronger as λ decreases.

Figure 7 illustrates the scattered field and total field for both TM and TE polarizations for the square PEC cylinder with $\lambda = D/2$ ($D = 0.5$m). These field distributions are similar to that from the cylinder with $\lambda = R$ as shown in Figure 5 due to similar ratios of dimension to wavelength. Figure 8 shows the scattering results for the circular cylinder with an irregular cross-section as shown in Figure 3 which has no analytical solutions for the field distributions. The scattered fields E_z^{sc} and H_z^{sc} from the irregular cylinder on the left side ($x < 0$) are much less than that from the circular and square ones due to relatively small dimension on the left side of the irregular shape.

For all three PEC cylinders with different cross-sections, the electric fields E_z decrease significantly behind the PEC cylinders ($x > R$ or $D/2$, $-R < y < R$ or $-D/2 < y < D/2$), since the PEC cylinders behave like shields, as expected.

3.2 Analytical solutions for circular conducting cylinder

The analytical solutions for the scattering by a circular conducting cylinder can be obtained for both TM and TE waves. Applying wave transformation, the TM incident plane wave can be given in terms of cylindrical waves [1]:

$$E_z^{\text{inc}}(r,\phi) = E_0 \sum_{p=-\infty}^{\infty} j^{-p} J_p(kr) e^{jp\phi} \tag{29}$$

where E_0 is constant and ϕ is the positive angle from the x axis. Applying the boundary condition on the PEC cylinder Γ_0, the TM scattered field for the circular conducting cylinder can be given by [1]:

$$E_z^{\text{sc}}(r,\phi) = -E_0 \sum_{p=-\infty}^{\infty} j^{-p} \frac{J_p(kR)}{H_p^{(2)}(kR)} H_p^{(2)}(kr) e^{jp\phi} \tag{30}$$

where R is the circular radius of the cylinder. Similarly, the incident and scattered fields for TE-polarized waves can be given as:

$$H_z^{\text{inc}}(r,\phi) = H_0 \sum_{p=-\infty}^{\infty} j^{-p} J_p(kr) e^{jp\phi} \tag{31}$$

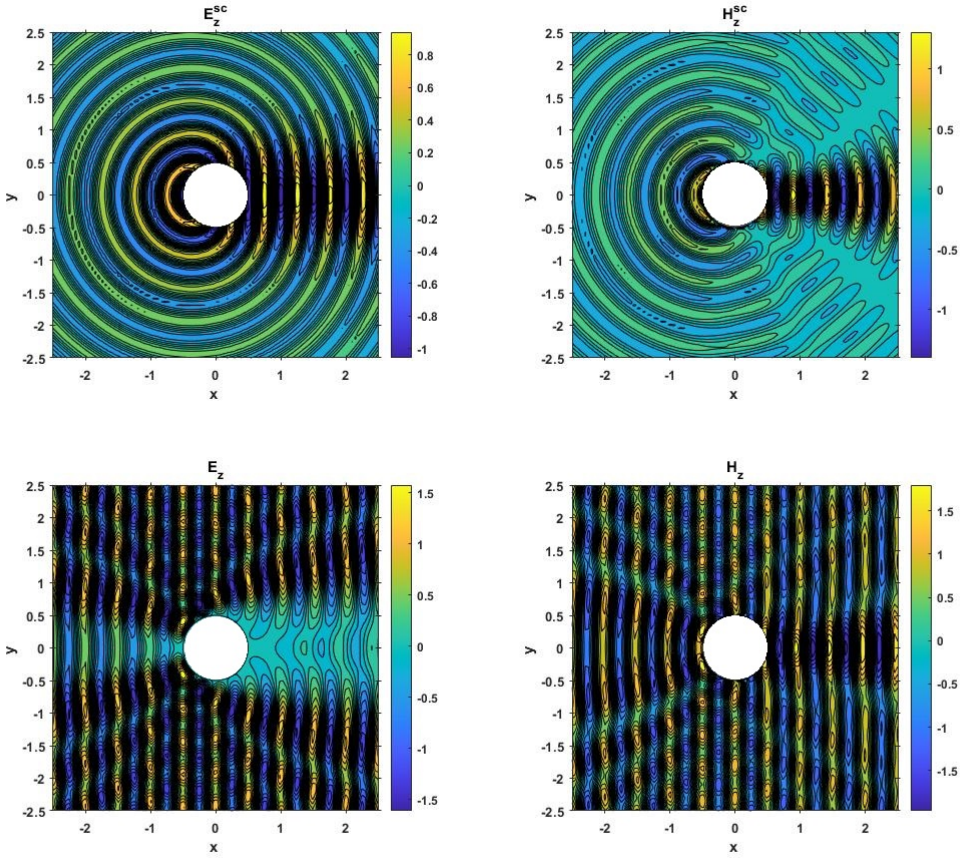

Figure 5: MoM results of scattered fields (E_z^{sc} and H_z^{sc}) and total fields (E_z and H_z) for circular PEC cylinder with $\lambda = R$.

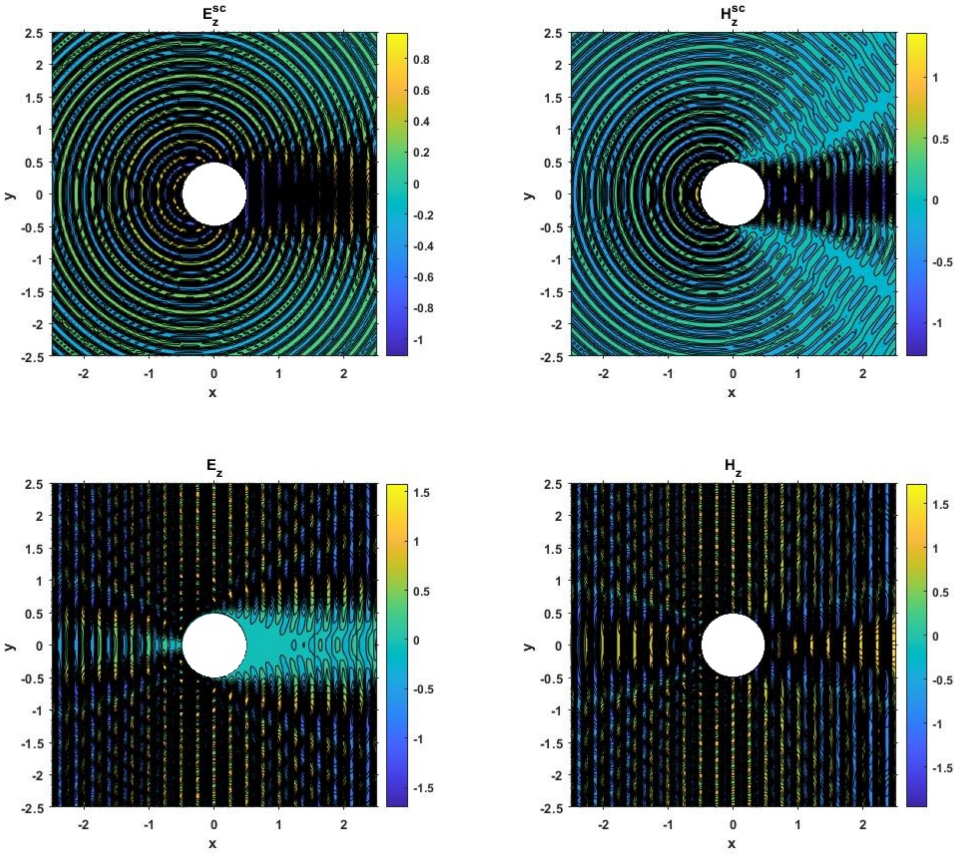

Figure 6: MoM results of scattered fields (E_z^{sc} and H_z^{sc}) and total fields (E_z and H_z) for circular PEC cylinder with $\lambda = 0.5R$.

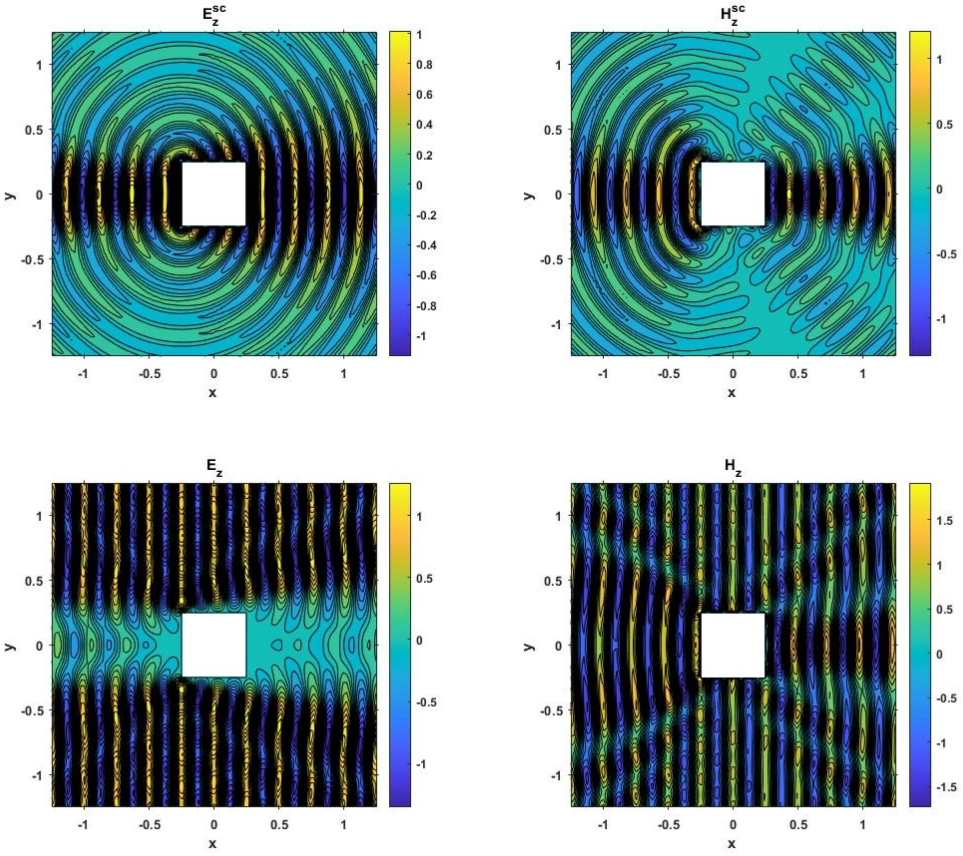

Figure 7: MoM results of scattered fields (E_z^{sc} and H_z^{sc}) and total fields (E_z and H_z) for square PEC cylinder with $\lambda = D/2$.

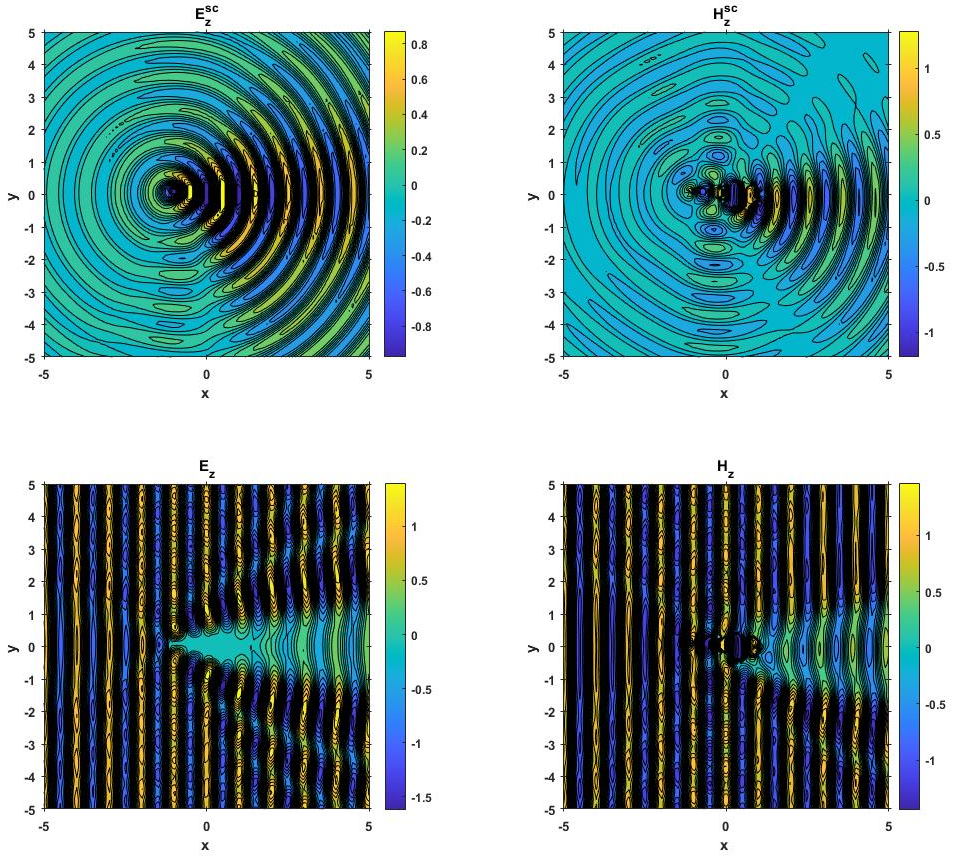

Figure 8: MoM results of scattered fields (E_z^{sc} and H_z^{sc}) and total fields (E_z and H_z) for the irregular PEC cylinder (as shown in Figure 3) with $\lambda \approx$ the largest dimension of the object in y direction (couldn't really exclude the irregular object from the figures).

$$H_z^{sc}(r,\phi) = -H_0 \sum_{p=-\infty}^{\infty} j^{-p} \frac{J_p'(kR)}{H_p^{(2)'}(kR)} H_p^{(2)}(kr) e^{jp\phi} \tag{32}$$

where H_0 is a constant, $J_p'(z)$ and $H_p^{(2)'}(z)$ may be evaluated by using the identity [2]:

$$A_p'(z) = -A_{p+1}(z) + \frac{p}{z} A_p(z) \tag{33}$$

where A denotes J and $H^{(2)}$. Here, we nondimensionalize the four fields in (29)-(32) by dividing each of them by E_0 or H_0 correspondingly for comparing to the MoM results.

Using p = -80 to 80 for the above four equations, one may obtain converged results for the wave transformation [1]. Figure 9 and Figure 10 show the analytical solutions for $\lambda = R$ and $\lambda = 0.5R$, respectively. Overall, we obtained a good agreement between the MoM and the analytical solutions for both TE and TM polarizations and both $\lambda = R$ and $\lambda = 0.5R$. This compassion validates the MoM developed in this work for modeling the scattering fields by an infinitely long PEC cylinder.

4 Conclusion

In this project, we developed a 2D MoM approach to simulate the TM and TE scattering from an infinitely long PEC cylinder of different cross-sections. We considered three cross-sections of the PEC cylinders that are circular, square, and irregular. The MoM developed in Matlab for modeling both TM and TE polarizations is strictly based on the 2D electric field integral equation (EFIE) and magnetic field integral equation (MFIE) introduced in [1]. The *pdetool* in Matlab was used to generate discretized segments on the boundary of each cylinder cross-section.

We validated the MoM results by comparing the scattered and total field distributions for both TE and TM polarizations to analytical solutions for the circular PEC cylinder with different radii. Overall, a good agreement between the MoM and analytical solutions was obtained. The presented approach may be easily used for other infinitely long PEC cylinders with various cross-sections.

Future studies may include evaluating the *scattering width* for scattering analysis for cylinders with various cross-section [1]. This parameter calculated from (30)-(32) considering far field ($k_0 r \to \infty$) for circular cylinders could help to validate the results from the MoM. Future studies could also extend the MoM to 3D for PEC scattering problems.

5 References

[1] J.-M. Jin, *Theory and Computation of Electromagnetic Fields*, 2nd edition. John Wiley & Sons,

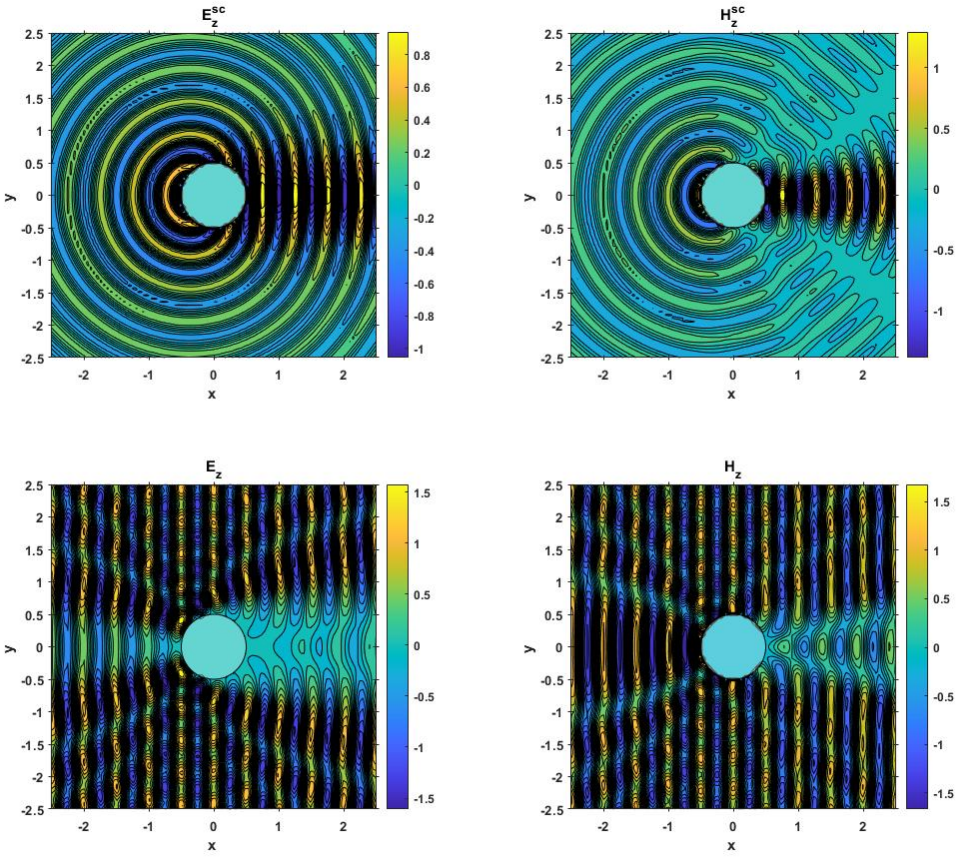

Figure 9: Analytical solutions of scattered fields (E_z^{sc} and H_z^{sc}) and total fields (E_z and H_z) for circular PEC cylinder with $\lambda = R$.

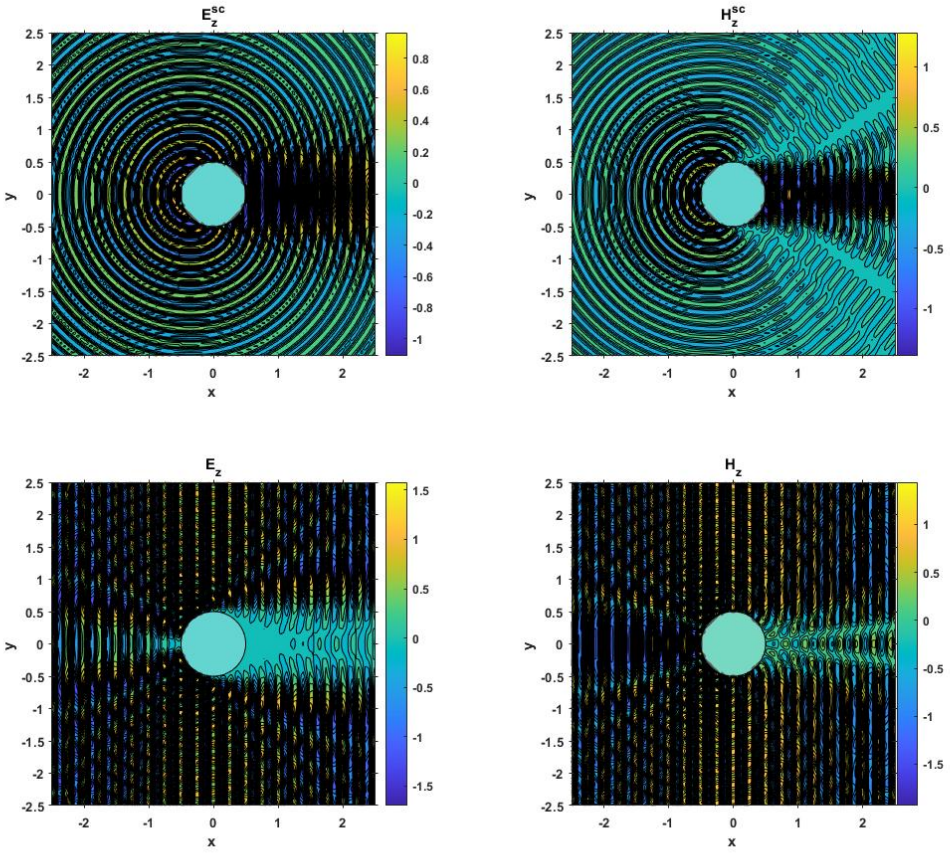

Figure 10: Analytical solutions of scattered fields (E_z^{sc} and H_z^{sc}) and total fields (E_z and H_z) for circular PEC cylinder with $\lambda = 0.5R$.

2011.

[2] *boost*. Accessed on: Dec. 11, 2021, [Online], Available: https://www.boost.org/doc/libs/1_57_0/*libs*/math/doc/html/math$_t$*oolkit*/*bessel*/*bessel*$_d$*erivatives.html*